AIAA JOURNAL
Vol. 38, No. 3, March 2000

Bifurcation, Limit-Point Buckling, and Dynamic Collapse of Transversely Loaded Composite Shells

Brian L. Wardle* and Paul A. Lagace†
Massachusetts Institute of Technology, Cambridge, Massachusetts 02139

The transverse-loading response of laminated composite shell structures is studied experimentally and numerically. Monolithic graphite/epoxy shell structures having layups of $[\pm 45_n/0_n]_s$ ($n = 1$, 2, and 3) closely represent commercial fuselage structures in both geometry and boundary conditions. A combined experimental and numerical approach is used to assess shell response to centered transverse loading. Experimentally, load-deflection response and mode-shape evolutions are measured and damage resistance characterized via dye-penetrant enhanced x radiography and sectioning. Nonlinear finite element analyses including buckling and dynamic collapse are conducted for comparison to the experimental data. Modeling results allow a more refined interpretation of observed bifurcation phenomena, particularly premature transition to a secondary equilibrium path attributed to geometric imperfections. A novel finite element technique introduced in previous work is found to be superior to traditional methods for identifying and traversing bifurcation points in this work. A simply supported axial boundary condition is found to give a much more complex buckling response (bifurcation and limit-point buckling, as well as dynamic collapse) than specimens with a free axial edge (bifurcation or limit-point buckling). Experimental and numerical comparisons for the range of thicknesses considered indicate that elasticity of the in-plane boundary condition and transverse shear effects need further consideration. Observed shell damage is typical of that observed for composite plates. Results of this work give new insight into the response of composite fuselage panels to damaging transverse events, particularly in regard to instability/buckling behavior.

Introduction

DAMAGE resistance and tolerance of fibrous composite structures are of significant concern to the aerospace community because of the relatively low through-thickness strength and susceptibility of these structures to damaging events, e.g., impact caused by tooldrop or birdstrike. In the area of damage resistance, the transverse loading of composite plate structures has been studied extensively, whereas relatively little work has been completed with composite shells.[1–3] Distinct differences in plate and shell structural response[4–9] and/or damage mode and extent[7,10,11] have been observed and linked to shell buckling. Because of these observed differences in plate and shell damage resistance characteristics, there is a substantial need to better characterize/understand shell response (particularly buckling) to transverse loading in order to better address damage tolerance concerns for composite aerospace structures (e.g., wing and fuselage).

Transversely loaded composite shell response involves nonlinear geometric/kinematic couplings, large rotations, and also buckling. Analytical and numerical studies, particularly finite element analyses, have sought to characterize the elastic response of isotropic and composite shells to static transverse loading, e.g., Refs. 4 and 12–17, and also to impact, e.g., Refs. 4, 9, 18, and 19. The static response is of interest because quasi-static testing of composite plates and shells oftentimes gives a response, including damage state, equivalent to impact loading.[20–28] Previous numerical work has focused on calculating the limit-point buckling response, which is characterized by similar (and symmetric) pre- and postbuckling deformation modes. Recent experimental and numerical work has shown that for these types of shell structures, bifurcation buckling must also be considered.[11,29–32] Bifurcation is characterized by dissimilar prebuckling (symmetric) and postbuckling (asymmetric) deformation states. In the response of arches, bifurcation involves a transition from a primary path (deformation mode symmetric with respect to the arch center) to a secondary path (deformation mode asymmetric, or inextensional[33,34]). Recent experimental and numerical work shows that bifurcation plays a key role in the response of transversely loaded shells.

The objective of the present work is to understand better composite shell response (particularly buckling and damage resistance) to centered, transverse loading through experimentation and finite element modeling. The geometry and loading are of interest because of low-velocity impact damage concerns to primary aircraft structures such as the fuselage of a commercial transport. Finite element modeling was undertaken to give additional insight into the experimental shell response, including damage resistance. The measured response, particularly buckling phenomena, can be more clearly understood by comparison to elastic buckling predictions from the finite element models. Finite element comparisons to the measured response also give insight into modeling assumptions, which need to be further refined to obtain a true predictive capability for damage resistance. Within the combined experimental/numerical framework, the effect(s) of changing shell thickness and boundary conditions on the response are particularly studied. Results using boundary conditions from a typical (plate and shell) test configuration[30–32] and those representing a fuselage section are compared to facilitate a better understanding of a realistic structural response to a transverse loading event. Shell thickness has been shown in previous work to strongly affect the buckling and damage response of composite shells[7] and is further explored herein with the more realistic configurations (boundary conditions). Through these specific explorations, a better understanding of the transverse-loading response, particularly damage resistance, of fuselage-like composite shells can be attained.

Approach

Because of complexities in the loading and the existence of discontinuities, it is difficult to study damage issues by direct analysis of a specific full-scale aerospace component such as a fuselage or wing. Therefore, it is desirable to obtain a more general understanding of

Received 12 February 1999; presented as Paper 99-1322 at the AIAA/ASME/ASCE/AAS/ASC 40th Structures, Structural Dynamics, and Materials Conference, St. Louis, MO, 12–15 April 1999; revision received 3 June 1999; accepted for publication 4 June 1999.

*Postdoctoral Associate, Technology Laboratory for Advanced Composites, Department of Aeronautics and Astronautics; wardle@alum.mit.edu. Member AIAA.

†Professor and MacVicar Faculty Fellow, Technology Laboratory for Advanced Composites, Department of Aeronautics and Astronautics; pal@mit.edu. Associate Fellow AIAA.

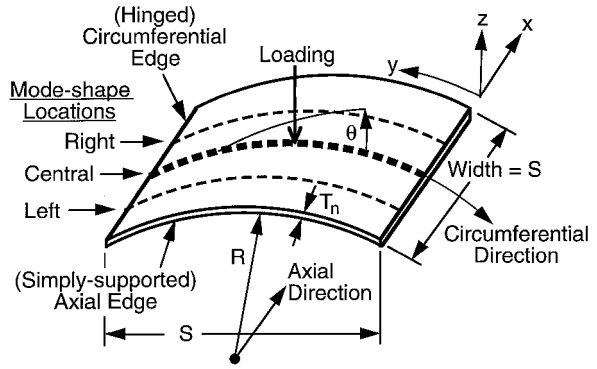

Fig. 1 Illustration of generic specimen showing radius, span, thickness (variable), ply angle, loading, boundary conditions, and locations for mode-shape evaluation.

damage issues via a much simpler structural element. The general understanding can then be applied to specific cases as appropriate. This simpler structure needs a proper resemblance to the actual structure in that it should have the same geometrical characteristics and loading conditions. With this in mind, a fuselage section is considered. This structural element is a singly curved cylindrical composite shell with a rectangular planform that has previously been investigated in experimental impact and quasi-static tests.[30,35] The static idealization is justified because of the equivalence of impact and quasi-static responses previously demonstrated for these types of structures and impact regimes of interest.[28] Thus, the transverse static loading of this structural element is studied in an effort to understand the shell response, particularly buckling and damage resistance.

The composite shells studied are manufactured from Hercules AS4/3501-6 graphite/epoxy prepreg tape in a $[\pm 45_n/0_n]_s$ layup. This layup and material system have been used previously in both damage resistance[7,11,28,30] and tolerance studies.[36] The orientation of ply angle θ with respect to the specimen axes and structural parameters is identified in Fig. 1. Individual plies have a thickness of 0.134 mm and are grouped to create effective plies. The scaling parameter n takes on the values 1, 2, and 3 to give three different laminate thicknesses: 0.804, 1.608, and 2.412 mm (6, 12, and 18 plies, respectively). Specimens are designated by thickness T_n, where the subscript refers to the scale factor n. Geometric characteristics of the shells studied correspond to values for a commercial fuselage structure having a radius of 1.829 m (72 in.), span (stringer spacing) of 305 mm (12 in.), and width equal to the span (square planform).

The current work builds on previous work with similar composite shell structures,[31,32] which explored response differences, primarily caused by buckling, between composite plates and shells. In the current work, laminated composite shells with boundary conditions that closely represent a commercial transport fuselage section are studied. The idealized shell boundary conditions in this work are hinged (no in-plane sliding) along the circumferential shell edges and simply supported (in-plane sliding allowed) along the axial edges as illustrated in Fig. 1. The true boundary condition of a fuselage section bordered by frames and stringers lies somewhere between simply supported and fully clamped. Thus, the boundary conditions used in this work are a reasonable idealization of a fuselage section.

Shell response in this work is evaluated both experimentally and numerically (finite element analyses). A test fixture used in previous work to create a hinged condition along the circumferential edges is modified to restrain also the shells along the axial edges (simply supported condition) while still maintaining the hinged condition. Load-deflection and mode-shape data are used to characterize the shell response. A series of two test types is used to study each specimen type (thickness): the first "load" test characterizes the overall specimen response up to failure or collapse, and the second "mode" test is used to obtain a detailed series of mode shapes at critical points in the specimen response. These critical points are determined from the load test of the same specimen type. Thus, a total of six specimens were tested. Mode-shape data acquired at three axial locations (see Fig. 1) are used to identify asymmetries in both the circumferential and axial shell directions. Damage resistance is experimentally characterized via x-radiography and sectioning to assess whether asymmetric (atypical) damage forms away from the loading site. Such damage has not previously been reported but has been hypothesized[32] because of the dominant asymmetric (bifurcation) mode that causes the maximum change in curvature along the shell to occur away from the loading site where damage typically forms for composite plate structures.

Nonlinear finite element models are used to predict the elastic structural response, particularly buckling behavior, of the composite shells. A key consideration in the finite element modeling is the prediction of limit-point vs bifurcation buckling from nonlinear prebuckling states. A novel asymmetric meshing technique (AMT) for inducing bifurcation in the finite element models[29,37] is used to assess bifurcation points and postbuckling behavior. The numerical shell models are used to interpret the experimental data better and also to assess modeling assumptions that need to be addressed in further work for these types of shell-buckling problems. Numerical and experimental results for the shells in this work (simply supported axial boundary condition) are compared with the response of the same specimen types with a free axial boundary condition[30,32] to determine the effect of the more realistic (fuselage) boundary condition on the resulting response.

Experimental Specifics

An overview of the experimental procedures is given in this section. Detailed information on the experimental procedures can be found in Ref. 29.

Specimen Preparation

Shells were manufactured using standard layup and cure procedures for this material system,[38] except that the laminates were cured on specially designed cylindrical molds. Laminates were laid up by hand and processed using the standard manufacturer's cure cycle of a 1-h flow stage at 116°C and a 2-h set stage at 177°C. This was conducted in an autoclave under vacuum with 0.59 MPa external pressure. Laminates were postcured in an oven at 177°C for 8 h and subsequently cut to the desired dimensions using a water-cooled diamond-grit cutting wheel. Final specimen dimensions after cutting are 305 mm (12 in.) spanwise and 314 mm ($12\frac{3}{8}$ in.) widthwise. The width is slightly greater (9.53 mm) than the span because the shells displace in-plane (x direction in Fig. 1) during testing at the axial simple-support boundary condition. The black composite shells are painted with flat-white spray paint using the procedure established previously,[29,30] as required by the laser transducer that measures deflection mode shapes.

An evaluation of the manufacturing technique for the specimens in this work shows that the specimen quality (radius and thickness) is acceptable. Thickness and radius values averaged over all specimens are within 3% (thickness) and 7% (radius) of the nominal values with acceptable coefficients of variation (less than 4% for both thickness and radius). Average measured radius and thickness values for each specimen in this work are provided in Table 1 along with the percent difference from the nominal values.

Test Fixture

The shells were restrained in a test fixture that approximates boundary conditions of pinned/no in-plane sliding (hinged) on the circumferential edges and simply supported on the axial edges

Table 1 Radius and thickness data

	Radius		Thickness	
Specimen[a]	Average, mm	Difference, %[b]	Average, mm	Difference, %[b]
T_1 load	1978	+8.2	0.822	+2.3
T_1 mode	1959	+7.1	0.836	+3.9
T_2 load	1942	+6.2	1.634	+1.6
T_2 mode	1968	+7.6	1.526	−5.1
T_3 load	1959	+7.1	2.493	+3.4
T_3 mode	1915	+4.7	2.334	−3.2

[a]Indicates specimen type (thickness) and test type.
[b]Indicates percent difference from the nominal value.

(in-plane refers to the curvilinear shell plane, x and y directions in Fig. 1). A specially designed test fixture from previous work[11,30,35] was modified for use in this work, preserving many of the essential features. The original fixture provided hinged circumferential edges for both shallow and deep shells, but allowed free axial edges. This fixture was modified by adding supports to the axial edges to achieve the simply supported condition desired in this work. On each shell edge the axial support consists of upper and lower restraints that make contact with the upper and lower surface of the 1.829-m (72-in.) radius shell edge. The upper and lower axial restraints contact the shell via knife edges with rounded corners having radius of 4.76 mm ($\frac{3}{16}$ in.). The edge of the axial shell rests between the upper and lower knife-edge restraints so that transverse displacement (z direction in Fig. 1) is restricted, but rotation and in-plane displacement (x and y directions) are allowed. Further details of the specimen setup and placement in the test fixture can be found in Ref. 29.

Quasi-Static Testing and Mode-Shape Measurement

Two types of testing were conducted: load tests to assess the overall loading response and mode tests, which give detailed mode-shape evolutions. The load tests are performed first to characterize experimentally the loading response over the entire regime of interest. The regime of interest includes all behavior until an instability is observed or until large-scale damage is observed. Instabilities are observed during testing by monitoring a real-time plot of load vs elapsed test time. As stroke increases linearly during the test, this is equivalent to observing a load-deflection plot. Instabilities are indicated by a gradual reduction in the slope of the load vs time plot until the load decreases. Damage formation is indicated by loud cracking and popping noises during testing as well as the formation of visible matrix cracks on the painted concave surface of the shell directly under the indentor. In the mode tests the stroke is held at predetermined positions so that mode shapes can be assessed. The stroke (center deflection) positions are determined using load-deflection data from the load tests such that a sufficient number (typically six or seven) of evenly spaced mode shapes are acquired to characterize the shell (buckling) response. Additional mode shapes are considered if interesting points are identified on the initial (load test) load-deflection plots.

All tests are run in stroke control on an MTS-810 uniaxial hydraulic testing machine with an Instron 8500+ digital controller. Stroke resolution on the controller is 10 μm. Shells are loaded using a 12.7-mm-($\frac{1}{2}$-in.)-diam hemispherical steel indentor. Load is acquired with a PCB model 208A04 22240 N (5000 lb) force transducer with resolution of 0.09 N (0.02 lb). Discretization of the analog data by the A/D board limits the recorded load resolution to 0.27 N (0.06 lb) but does not limit the stroke resolution of 10 μm. A stroke rate of 0.05 mm/s is used for both loading and unloading with a data (load and stroke) sampling rate of 1 Hz to allow the tests to proceed quasistatically and the response to be adequately characterized.

A noncontacting laser transducer with resolution of 10 μm is used to survey shell-deflection mode shapes during testing. The laser shines against the concave painted surface of the shell with a beam spot of 1 mm in diameter. The laser is mounted on a traverse assembly specifically designed to assess mode shapes during testing of shells.[30] The traverse has continuous movement in the spanwise (shell) direction and discrete axial positions in 12.7-mm ($\frac{1}{2}$-in.) intervals. Mode shapes were evaluated at three axial locations: along the axial centerline (directly under the indentor) and at 76.2 mm (3 in.) on either side of the centerline (see illustration in Fig. 1). The discrete axial location of the laser is known at all times but the spanwise position, being the direction of continuous movement, is measured using a rack-and-pinion system connected to a potentiometer, which provides a linearly varying voltage with spanwise position. Using the data acquisition system already described, the spanwise position is known within 0.5 mm and the shell height within 10 μm.

Damage Evaluation

All specimens were evaluated for damage after testing using x-radiography[39,40] and sectioning/microscopy. After each test is complete, a 0.79-mm-($\frac{1}{32}$-in.)-diam hole is drilled through the thickness of the specimen at the center of the loading site. Flash tape is applied to the concave side of the specimen, and a dye is injected with a syringe into the hole on the convex surface. The x-ray opaque penetrating dye is 1,4 diiodobutane (DiB), which seeps into cracks and delaminations in the specimens through capillary action. Dye-penetrant enhanced x-radiography provides a view of the damage state, typically matrix cracks and delaminations, that is integrated through thickness. DiB-soaked portions of the shell specimens, where the dye has soaked into matrix cracks and delaminations, show up as dark areas in the x rays. A sample x-ray photograph showing a large delamination is provided in Fig. 2. The x-ray photograph is of the damage state looking down at the convex side of the shell. The large damage (delamination) axis is along the 45-deg ply with a smaller delamination at -45 deg. The small, light, circular region at the center is the hole for injecting the dye, and the dark line at 45 deg is a long matrix split in the ply on the concave side of the shell. Shorter matrix splits can also be seen at -45 and 0 deg. X radiographs are a planar projection of a curved surface resulting in a smaller damage length in the photograph. This reduction in damage length is less than 0.2% in the circumferential direction (maximum effect), which is negligible.

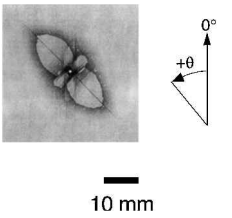

Fig. 2 Sample planar x radiograph showing damaged region and ply orientation.

Sectioning gives through-thickness damage details and provides a means for investigating damage away from the loading site. Specimens were cut with a diamond-grit wheel into four sections at the three axial locations where the mode shapes are evaluated. The sectioned axial edges are then polished with a rotating felt bob using a slurry of 0.5-μm grit and water. This creates a surface needed to identify through-thickness damage with a microscope using a magnification of 30–40 ×. Matrix cracks appear as light lines through the darker matrix, and delaminations appear as lightened areas between plies (or ply groups) and are clearly visible in the region of loading.

Finite Element Analysis

Numerical work in this investigation focuses on predicting the nonlinear elastic response of shells with particular attention to both bifurcation and limit-point buckling. Previous analyses of similar shells have focused solely on limit-point analyses of shells with free axial edges, e.g., Refs. 4, 8, 12–17, 19, and 41–44. Only recently has bifurcation buckling been considered along with limit-point buckling for these shell geometries using a novel technique for inducing bifurcation within nonlinear finite element analyses.[29,37] The AMT[37] is used in this work to assess bifurcation using the STAGS finite element code available at the Structural Materials Branch of NASA Langley Research Center.[45] STAGS is used extensively to analyze the nonlinear response and stability of composite shell structures.

The 410 shell element available in STAGS is used for its applicability to the thin-shell structures in this work.[46] This workhorse element in the STAGS code employs the nonlinear Kirchhoff–Love shell hypothesis that ignores transverse shear. However, it is known to be extremely accurate for modeling thin-shell structures. It is a displacement-based, four-node, quadrilateral, C^1 shell element having a cubic (translations and rotations) bending field and a linear/cubic (in-plane translation/transverse rotations) membrane field. The 410 element has three translational and three rotational degrees of freedom per node and also includes drilling rotational stiffness. The true Newton capability within STAGS is used to solve iteratively the resulting nonlinear equations. Arbitrarily large rotations, but small strains, are modeled using the standard corotational procedure[41] in STAGS, and limit points are easily traversed using the Riks arc-length procedure.[47]

Quarter- or half-symmetry was not assumed in this work because a full model of the shell is required to investigate bifurcation, i.e.,

Table 2 AS4/3501-6 ply data

Property	Value
E_{11}	142 GPa
E_{22}	9.81 GPa
G_{12}	6.00 GPa
ν_{12}	0.3
ρ	1640 kg/m^3
Ply thickness	0.134 mm

symmetry is not present because of the asymmetric deformation mode associated with the bifurcation path. As discussed already, the AMT is used in this work to investigate bifurcation. Using the AMT, a numerical perturbation is introduced into the stiffness matrix of the shell model by meshing the structure asymmetrically. The resulting perturbed stiffness matrix in the nonlinear mathematical model acts to induce bifurcation in the same way as geometric and loading imperfections in traditional techniques. This allows the bifurcation response of the structure to be obtained directly, if it exists. Finite element results in this work using the AMT represent converged bifurcation or limit-point buckling solutions for the shells studied and have been validated by comparison to traditional techniques for inducing bifurcation.[29,37] Although the AMT solutions were confirmed by traditional techniques for evaluating bifurcation, these traditional techniques had difficulty identifying and traversing the bifurcation points in this work, whereas the AMT encountered no such problems. A complete formulation and discussion of the AMT is presented in Refs. 29 and 37. Shell discretization is summarized here: 20 elements and 17 elements in the axial and circumferential directions, respectively, are used to discretize specimen T_1; 20 and 19 elements, respectively, are used for specimens T_2 and T_3.

Effective laminate properties for the composite are computed within STAGS using the ply material properties given in Table 2. Experimentally determined values of radius (see Table 1) are used in the analysis along with nominal laminate properties, including thickness. Experimental and nominal values of width and span are identical because of the design of the test fixture. A right-handed, orthogonal, curvilinear coordinate system, as shown in Fig. 1, is used to identify the boundary conditions used in the analysis. Displacements (u, v, and w) and rotations (Rx, Ry, and Rz) are taken along/around the x, y, and z axes, respectively. The circumferential edge (hinged) constraint is represented in the model by setting all nodal displacements and rotations to zero ($u = v = w = Ry = Rz = 0$) except rotation about the x axis (Rx), where zero moment is enforced. The axial edge constraint is represented by setting the transverse displacement w and rotation about the x axis (Rx) equal to zero, whereas the other displacement and rotation degrees of freedom are unrestrained (zero force or moment). The shells are point-loaded in all cases at the center of the shell surface. Details of the loading used in the experiments, i.e., loading by a small (relative to shell dimensions) hemispherical indentor, were not included in the finite element models.

Results and Discussion

Experimental and numerical load-deflection and mode-shape evolutions are used in this work to describe the buckling behavior of the composite shell structures. In using these results, it is first useful to compare experimental results from the two test types (load and mode) conducted to understand the repeatability of the tests and thus establish that data from the two test types can be used interchangeably to describe a specimen's response. Following this, general characteristics of the shell-buckling response are discussed using both the numerical and experimental results. Thus, a general description and terminology for the shell response is provided, which subsequently is used in discussing effects such as thickness and boundary conditions on the resulting response. This section closes with a discussion of the damage resistance of the shell structures tested and implications of these results for further damage resistance studies.

Load- and Mode-Test Comparison

As already discussed, a total of six specimens were tested in this investigation in two types of tests: three thicknesses each tested in a load and mode test. A comparison of the loading and unloading response for these two test types is provided in Fig. 3 for specimen T_2. The load test in Fig. 3 was performed first to characterize the overall loading response of this specimen type. The initial softening and then nonlinear stiffening of the response is typical of that observed for shells in this work. Significant hysteresis in the unloading response is also typical and is expected based on previous work with similar composite shells.[30] Hysteresis is typically associated with damage and/or indentation formation at the loading site. Increased hysteresis in the load test is expected because this specimen was loaded to a higher peak force than the specimen in the mode test and thus has incurred more damage. The loading portion of the curve is noted to be quite similar in both test types except for small deviations from a smooth response in the mode test where stroke was held so that deflection mode shapes could be assessed. In the mode test in Fig. 3, mode shapes were taken at values of center deflection (stroke) of 2.0, 4.0, 6.0, 8.0, 12.0, and 16.0 mm. Deviations at held-stroke values were noted for all specimens. However, as found in previous work,[30] the load generally returns to the original path when loading recommences. These points are thus considered unimportant and are justifiably ignored in subsequent discussion.

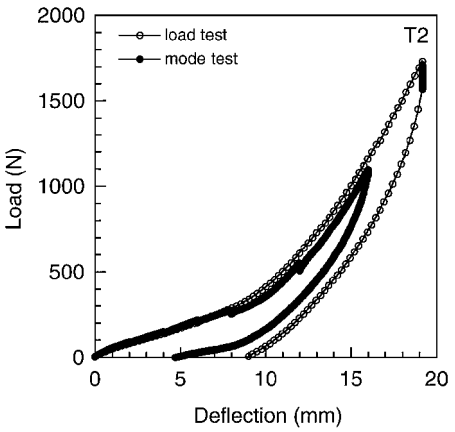

Fig. 3 Measured force-deflection response for specimen T_2 from load and mode tests.

The response comparison for specimen T_2 in Fig. 3 is typical of that for the other two specimen thicknesses considered in this work, i.e., apart from small deviations at the held-stroke positions in the mode tests, the response for the two test types is the same. Furthermore, mode shapes taken during the load tests are in excellent agreement with the mode-shape progression from the mode tests. (Note that mode shapes cannot be directly compared between the two test types because they were taken at different held-stroke positions.) Given the repeatability of the response for each specimen thickness, documented in detail in Ref. 29, mode-shape and load data from the load and mode tests are used interchangeably to describe the response of each specimen type (thickness) throughout this work.

General Shell-Buckling Characteristics

The finite element results presented in Fig. 4 for the load test of specimen T_1 serve to illustrate the range of nonlinear behavior and buckling phenomena observed in this work. The response of this shell is quite complex, involving nonlinear prebuckling, bifurcation, an unstable postbifurcation path, and dynamic collapse after a limit point. Consideration of the elastic response of this specimen illustrates shell-buckling phenomena and aids in the further discussion of the response of all specimens tested in this work.

Three stable equilibrium paths are marked in Fig. 4: the first (I) is the initial shell response involving symmetric deformations, the second (II) is a stable path that involves asymmetric (bifurcation) deformation modes, and the third (III) occurs after the shell reaches a limit point and collapses dynamically. The initial portion of the first equilibrium path (I) of specimen T_1 is nonlinear, with an initial softening response below 2 mm of applied center deflection followed by a stiffening response until the bifurcation point at a center-deflection

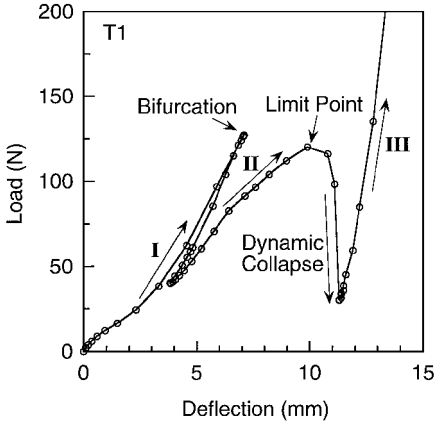

Fig. 4 Predicted load-deflection response for specimen T_1 showing bifurcation, limit-point buckling, dynamic collapse, and three (stable) equilibrium paths (I, II, and III).

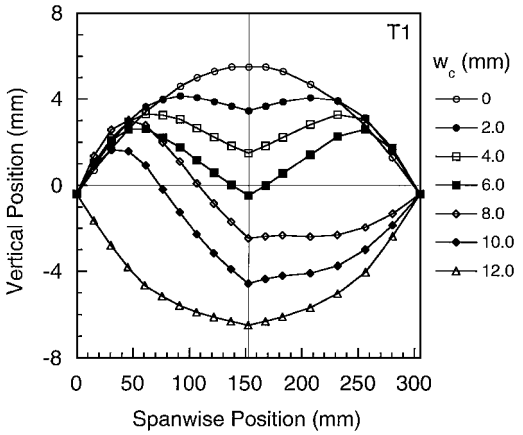

Fig. 5 Predicted central spanwise deformation modes for mode test of specimen T_1 at different values of center deflection w_c.

value of 7.1 mm. Prior to bifurcation, shell deformation is characterized by deformation modes that are symmetric with respect to the loading (shell center) in the circumferential (spanwise) direction as illustrated in the central mode-shape evolutions in Fig. 5. At the critical point the shell bifurcates to an unstable path associated with asymmetric mode shapes. The unstable path is characterized by decreasing load and deflection at the loading point, but has associated with it increasing amplitude of the asymmetric deformation mode. This path would thus not be found in a deflection- or load-controlled experiment because it is unstable for both of these loadings. It is possible to evaluate this path in the finite element analysis because of the path-parameter algorithm used to increment the loading, i.e., a combination of load and deflection control are used in the analysis to obtain this unstable path.

The asymmetric bifurcation mode associated with bifurcation is very similar to the well-known inextensional mode in simple arch analyses[34] and can be clearly distinguished in the central spanwise mode shape at a center-deflection value of 8.0 mm in Fig. 5. (Note that the mode at a center-deflection value of 6.0 mm is on the first equilibrium path and not the unstable or secondary paths.) The unstable bifurcation path lies very close to the primary (I) equilibrium path and is noted to decrease in both load and deflection from the bifurcation point to approximately 40 N and 3.8 mm, respectively, in Fig. 4. At this point the response resumes loading on a second stable equilibrium path (II) that leads to a second critical point. This second critical point is a limit point and is not associated with bifurcation (no eigenvalues are indicated at this point in the analyses). Limit points are typically associated with nonlinear collapse involving only symmetric (pre- and postbuckling) deformation states. However, at the limit point in Fig. 4, both asymmetric and symmetric modes are present because bifurcation occurs before the limit point is reached

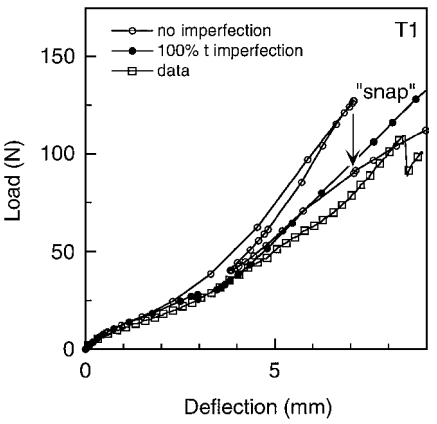

Fig. 6 Comparison of experimental and numerical load-deflection results for load test of specimen T_1. Numerical results incorporating an asymmetric spanwise geometric imperfection show direct transition from the first to the second equilibrium path.

(see mode at center-deflection value of 10.0 mm in Fig. 5). After reaching the limit point, the shell collapses dynamically to the final (tertiary, III) equilibrium path, which corresponds to a fully inverted configuration as illustrated by the mode at a center-deflection value of 12.0 mm in Fig. 5, i.e., the convex shell collapses into a concave configuration. In this region of dynamic transition, shell inertia must be accounted for in a fully dynamic analysis wherein the equations of motion for the shell are integrated in time. This was done in the current work.

Load-deflection data from the load test for specimen T_1 are compared with the finite element results in Fig. 6. Experimentally, the shell first experiences a period of load-softening below approximately 3 mm of applied center deflection. Above 3 mm, the response stiffens slightly until the load suddenly drops at a center-deflection value of 8.5 mm. At the load drop the shell audibly popped during testing, and the test was manually stopped and held at 8.9 mm of deflection to take mode-shape measurements before the specimen was unloaded. As this specimen was undamaged internally (sectioning and x radiography), the sudden load drop and associated popping is attributed to dynamic buckling at a critical point. This same critical point is also evident in the loading and unloading portion of the load-deflection response for the mode test of specimen T_1. In the numerical results for specimen type T_1 (see Fig. 4), bifurcation involves an unstable postbifurcation region wherein both load and deflection decrease simultaneously. In stroke (deflection) control, such as that used in the experiments, the shell would dynamically snap at the bifurcation point directly to the stable second equilibrium path, consistent with increasing the deflection at the loading point. Ignoring dynamic effects, an ideal deflection-controlled snap is illustrated in Fig. 6, using the numerical results from the load test of specimen T_1.

Comparison of the experimental and numerical results allows a much clearer interpretation of the observed shell-buckling behavior of specimen T_1. Whereas the initial portion of both responses correspond in Fig. 6, the experimental response departs from the model results prior to the predicted bifurcation point in Fig. 4 and appears to follow the second equilibrium path from its initiation at a center-deflection value of 3.8 mm (or a load of 40 N). It is hypothesized that the test specimen bifurcates directly to the predicted second (II) equilibrium path, likely because of loading or geometric imperfections as has been suggested for similar cases.[48–50] This interpretation can be confirmed because of the mode-shape data acquired in the experiments. Considering the experimental mode-shape data provided in Fig. 7 and the numerical mode shapes in Fig. 5, the test specimen is noted to bifurcate between center-deflection values of 2.0 and 4.0 mm. This is consistent with joining the second equilibrium path, rather than continuing along the primary equilibrium path associated with symmetric deformations. A spanwise geometric imperfection in the form of the asymmetric bifurcation mode (maximum amplitude equal to one shell thickness) included in the finite element model induces precisely this transition as shown in

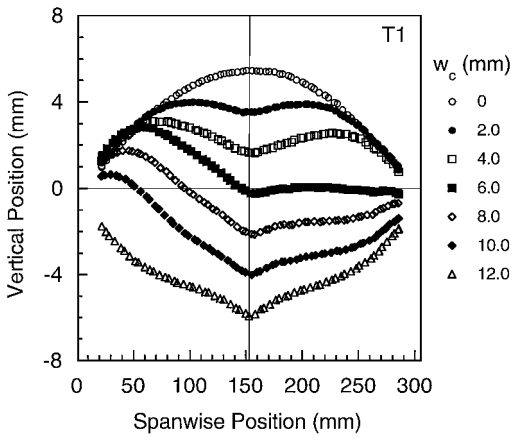

Fig. 7 Measured central spanwise deformation modes for mode test of specimen T_1 at different values of center deflection w_c.

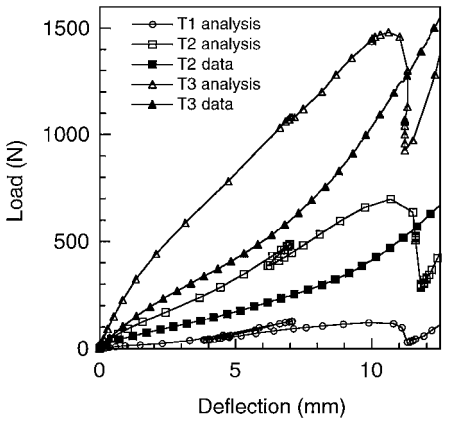

Fig. 8 Numerical and experimental load-deflection results for specimens with different thickness.

Fig. 6. Therefore, because of the comparison with numerical predictions, the observed response of specimen T_1 is understood to bifurcate in a stable manner to an adjacent equilibrium path (secondary equilibrium path, II) rather than continue along the primary path (I).

Effects of Geometry and Boundary Conditions

In previous experimental work with similar composite shells, varying thickness has been shown to affect strongly the initial and overall (secant) stiffness of the structures tested because of its contribution to both bending and membrane stiffness of the shell.[7] Numerical load-deflection responses for the three specimens, as well as experimental results for specimens T_2 and T_3, are presented in Fig. 8 for comparison. It is immediately obvious that thicker panels, as expected, are stiffer both initially and overall. Both the load and deflection range associated with the bifurcation point (instability region) decreases significantly with thickness, as can be noted by comparing the numerical responses of specimens T_1 and T_2. This instability region associated with the bifurcation point disappears altogether in the numerical response of specimen T_3. The deflection associated with the critical points at both the first bifurcation point and the second critical (limit) point are noted to be approximately independent of thickness. Bifurcation occurs at a center-deflection value of approximately 7.0 mm, and the second local maximum occurs at a value of approximately 10.5 mm for all specimen types in the numerical work. However, the loads associated with these points clearly increase with increasing specimen thickness. The consistent values of deflection associated with buckling for specimens of different thickness have been noted in previous work with arches (e.g., Ref. 51) and is related to the typical shell-height parameter. As a result, shell height is oftentimes used to nondimensionalize transverse deformations of arches and shells, e.g., Refs. 5 and 52. Nominal shell height for the shells in this work is 6.4 mm, which is slightly less than the displacement corresponding to bifurcation (7.0 mm). However, the out-of-plane deformations vary from a maximum at the shell center to zero at the restrained axial edges. Thus, these shells do not deform as arches, but they do share the geometric characteristic that buckling occurs at a constant value of center deflection approximately corresponding to the shell height.

A characteristic of the experimental data relative to the numerical predictions is that the data generally represent a more compliant response. (See the numerical and experimental load-deflection results in Figs. 6 and 8.) The experimental response is in good agreement with the numerical results for the thinnest specimen (T_1), as shown in Fig. 6, but the experimental and numerical results diverge at higher loadings, as shown in Fig. 8. Buckling is not evident in the load-deflection data for the two thicker specimens (T_2 and T_3), nor is an asymmetric bifurcation mode observed in the mode-shape evolutions even though bifurcation is predicted in the numerical work (e.g., bifurcation is predicted to occur at a center-deflection value of 7.1 mm in Fig. 8 for specimen type T_2). These observations are consistent with findings in previous work with composite shells having free axial edges[29,31] and can be understood with regard to modeling assumptions. The analysis does not include transverse shear or account for experimental realities such as compliance of the test fixture (elastic, not rigid, circumferential boundary condition), contact behavior at the loading point, or damage. All of these effects act to make the experimental response more compliant than the numerical results, as well as delaying or eliminating bifurcation entirely. The trend of increased compliance (and disagreement) between the experimental and numerical results as thickness increases is caused by a decrease in relative stiffness of the test fixture as compared to that of the shells, deformation at the loading site caused by shear, and/or damage. The magnitude of the compliant effect, coupled with previous work considering the effect of transverse shear on the transverse loading response of composite shells[14] and lack of damage in some cases, indicates that test-fixture compliance is the most reasonable explanation for the observed numerical/experimental disagreement. However, all three modeling assumptions need further explicit consideration from a relative perspective and are recommended for future work.

A secondary effect of the experimental boundary conditions, this time a contribution from the axial supports (simple-support boundary condition), is also noted with regard to deformation-mode asymmetries in the axial direction. Experimental and numerical left and right spanwise mode shapes for specimen type T_1 are provided in Figs. 9 and 10, respectively, to illustrate this response characteristic. As with the central spanwise mode shape, bifurcation is clearly evident in the experimental asymmetric left and right spanwise modes beginning at a center-deflection value of 6.0 mm. Comparing the left and right predicted modes in Fig. 10, these modes are noted to be quite similar apart from a small spanwise asymmetry in each mode, which is noted to be axially antisymmetric with respect to the shell center (loading point). This axial antisymmetry has been previously discussed for composite shells of this type and is attributed to bending-twisting coupling in the composite laminate[31,32] (i.e., if the shell were isotropic, the left and right modes would be identical). Apart from the slight axial antisymmetry observed in all left and right mode-shape comparisons, the left and right numerically evaluated modes are similar, i.e., there is symmetry in the axial direction. However, the experimental modes in Fig. 9 do not show this same agreement directly after bifurcation. This is clearly evident in the mode at a center-deflection value of 10.0 mm, where the right mode indicates that the shell edge (at the hinged boundaries) has snapped through to an inverted configuration, whereas the left mode has not inverted at the (left) boundary. Thus, an axial asymmetry, apart from the bending-twisting antisymmetry, is evident in the experimental data that is not predicted numerically. The hypothesis is made that imperfect axial boundary conditions, particularly frictional loading differences between the two axial boundaries, induce this axial asymmetry.

Effects of the axial boundary condition (free vs simply supported) are assessed directly by comparing experimental and numerical load-deflection responses. Experimental data for specimens with free axial edges have been reported previously.[32] The experimental and numerical loading responses for specimen type T_1, using the

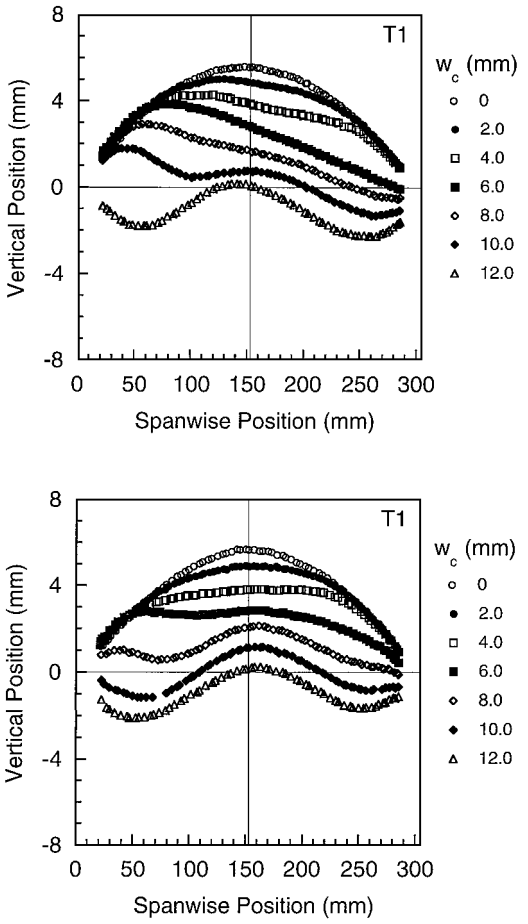

Fig. 9 Measured left (top) and right (bottom) spanwise deformation modes for mode test of specimen T_1 at different values of center deflection w_c.

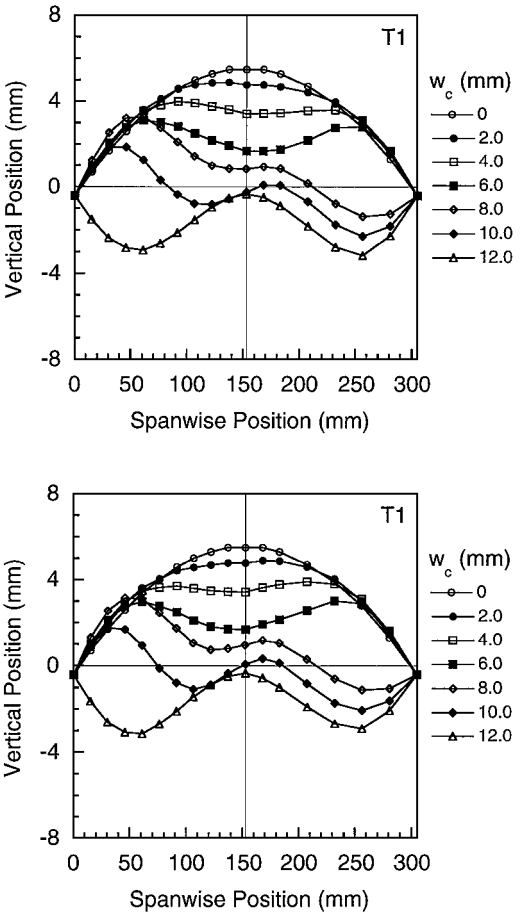

Fig. 10 Predicted left (top) and right (bottom) spanwise deformation modes for mode test of specimen T_1 at different values of center deflection w_c.

two different axial boundary conditions, are presented in Fig. 11. The two experimental load-deflection responses display similar behavior prior to bifurcation of the unrestrained specimen at a center-deflection value of approximately 3.0 mm. Results from the numerical analyses for the same specimens also show similar behavior prior to bifurcation of the unrestrained specimen. The analysis shows that, in the region of loading prior to bifurcation, shells with these two different axial restraints deform similarly. This explains the similarity in the loading response prior to bifurcation. Similar behavior is generally noted prior to buckling for the other two specimen types (T_2 and T_3), with excellent agreement noted between the numerical responses prior to bifurcation. The unrestrained experimental loading response for these two thicker specimen types is noted to be slightly more compliant than the simply supported cases prior to bifurcation. The increased compliance (and disagreement) is more pronounced as thickness increases, as illustrated in the experimental load-deflection comparisons in Fig. 12 for specimen types T_2 and T_3. The hypothesis is made that this trend is also because of test-fixture compliance at the hinged (circumferential) edges. Test-fixture compliance in the circumferential direction would affect the axially simply-supported specimens less strongly because a percentage of the transverse load is reacted through the axial supports rather than entirely through the (compliant) hinged circumferential boundary.

The response comparison for specimen type T_1 in Fig. 11 is typical of those for the other two specimen types (thicknesses) with regard to differences caused by the axial boundary condition. The responses are similar prior to bifurcation for the unrestrained specimens, but the critical (bifurcation) loads for the simply supported specimens are noted to be much higher than for the unrestrained specimens, e.g., 127 N vs 25 N for specimen type T_1. The bifurcation point for the simply supported specimen has associated with it a secondary (bifurcation) path that is unstable in both load and deflection control. This is not observed for the unrestrained specimens that have a response (e.g., as in Fig. 11) that is unstable only in load-control. In the numerical results for axially simply supported shells in this work, bifurcation occurs from the first equilibrium path (symmetric deformation modes) to the second equilibrium path (asymmetric deformation modes) before collapsing at a limit point. In contrast to the axially unrestrained shells, asymmetric modes are associated with the limit point for the axially simply supported shells caused by the prior bifurcation. In both cases the shells reach an inverted configuration on a stiffening final (third) equilibrium path having associated symmetric deformation modes. In the unrestrained case the final path is the second stable equilibrium path, whereas for the simply supported cases this is the third stable path (caused by bifurcation and a limit point). In general, the response of the axially simply supported shells is more complex (bifurcation and limit-point buckling) and has higher critical loads than the response of shells with free axial edges.

Damage Resistance

A primary objective of this work with regard to composite shell damage resistance is to investigate the effect of bifurcation and the associated asymmetric deformation modes on the resulting damage. As already discussed, asymmetric and atypical (with regard to extent and distribution) damage states at the loading site have been observed for composite shells similar to those tested in this work.[11,28] Furthermore, the hypothesis has been made that asymmetric modes could lead to damage formation away from the loading site. This possibility is investigated in this work by sectioning the specimens at three axial positions and searching for damage.

Symmetric damage, typical of that observed for plates, is found through both sectioning and x-radiography techniques (see x radiographs in Fig. 13) for the shells in this work. The two thicker specimens that were damaged (T_2 and T_3) were not observed to

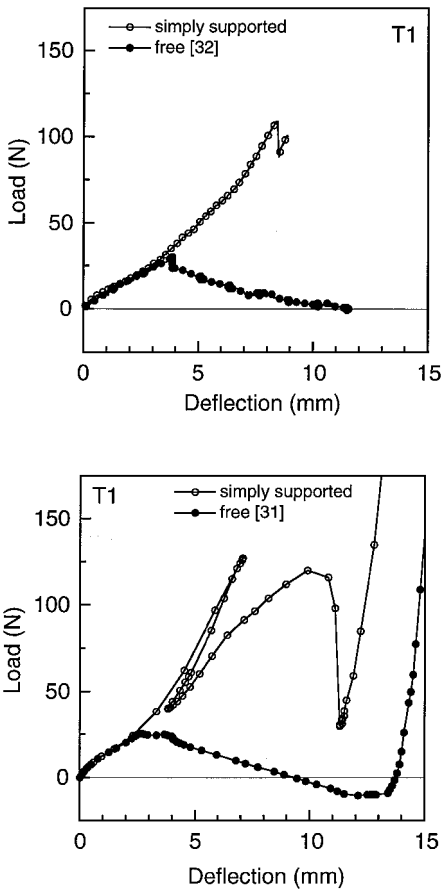

Fig. 11 Comparison of experimental (top) and numerical (bottom) load-deflection results for specimen T_1 with simply supported and free axial boundary conditions.

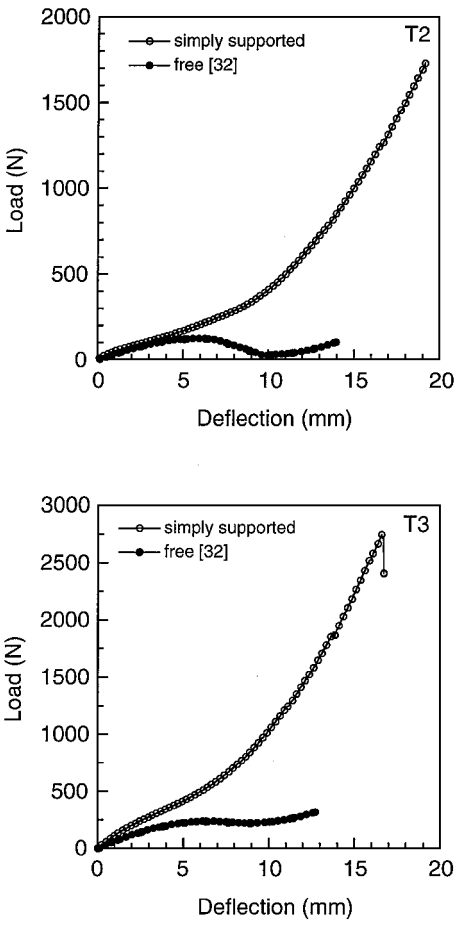

Fig. 12 Experimental load-deflection results for specimens T_2 (top) and T_3 (bottom) with simply supported and free axial boundary conditions.

bifurcate. Specimen type T_1, which was observed to bifurcate into asymmetric modes, was undamaged. Therefore, the specimens that did damage were not observed to bifurcate and thereby did not experience asymmetric modes. Atypical damage states at the loading site are thus not expected in such cases. Sectioning of specimen T_1 did not reveal damage formation away from the loading site. Thus, in regard to damage resistance, nothing atypical of that observed previously for composite plates of the same material and geometry is observed in this work. However, this result is certainly not conclusive based on the three specimen geometries considered in this work, i.e., the hypothesis of damage away from the loading site caused by asymmetric bifurcation modes has not been disproved. The mechanism for atypical damage formation (bifurcation into asymmetric modes) was observed; however, this specimen type T_1 was undamaged during testing.

The finding in the preceding section regarding loading-response agreement between axially free and simply supported shells has implications for damage-resistance testing of composite shells. Atypical damage found in previous work with composite shells was noted to occur on the first equilibrium path, likely because of the compressive membrane stress state on this path.[11] Investigation of this atypical damage is of considerable interest as it is the key difference between plate and shell damage resistance, i.e., it represents a significant area of composite damage resistance that is not well understood. Numerical and experimental results from this work indicate that the response for the axially unrestrained and simply supported shell configurations are similar in this region. Therefore, unrestrained (traction-free boundary condition) shells, which are straightforward to test relative to the simply supported configuration, are likely to provide damage resistance data that are applicable to the more realistic (fuselage or similar structure) case. However, this hypothesis requires further experimental evidence, particularly in regard to damage, because it is based solely on observed similarities in the loading response at this time.

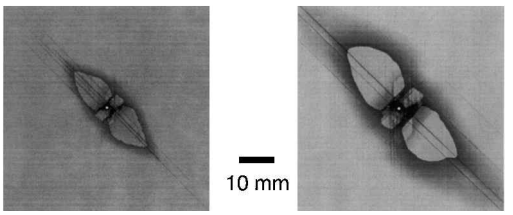

Fig. 13 X-ray photographs of specimen type T_2 (left) loaded to 1737 N (w_c = 19.1 mm) and specimen type T_3 (right) loaded to 2746 N (w_c = 16.6 mm).

Conclusions

The transverse loading response, particularly buckling and damage resistance, of several composite shell structures is investigated numerically (using finite elements) and experimentally in this work. The shells are monolithic laminated graphite/epoxy structures having geometric characteristics and boundary conditions representative of a commercial transport fuselage. Load-deflection and mode-shape results are used to characterize the composite shell response, which includes bifurcation, limit-point buckling, dynamic collapse, and three distinct stable equilibrium paths. The AMT is found to be quite effective in evaluating bifurcation from nonlinear prebuckling states for shells in this work. The effects of specimen thickness (three thicknesses) and axial boundary condition are particularly explored, as well as effects from compliance of the test fixture in the circumferential direction.

Whereas this investigation is limited to shallow, fuselagelike shells, the presence of bifurcation indicates that these shallow shells display a buckling behavior usually attributed to deep shells/arches. Bifurcation into asymmetric modes is easily identified in the shell response via mode-shape evolutions acquired during testing. These mode-shape evolutions, coupled with results from the numerical

modeling, allow a much clearer interpretation of the experimental loading response than would otherwise be possible. In particular, these comparisons allow a premature transition to an adjacent bifurcation path to be identified in the experimental data. Given the numerical results, the most probable explanation is that a geometric or loading imperfection (likely an asymmetry) induces the transition to the secondary path to occur early. This conclusion is supported by analysis wherein a geometric imperfection is included in the shell model and the early transition is achieved.

Comparison of the experimental and numerical load-deflection responses shows that, in general, the experimental response is more compliant than the predicted response. This is expected because of experimental effects such as transverse shear, damage, and test-fixture compliance, which are not included in the models. In particular, test-fixture compliance at the hinged circumferential boundary may induce a more compliant experimental response, delay or eliminate bifurcation, and promote a symmetric limit-point response. The effect of test-fixture compliance is more pronounced for thicker specimens because the relative stiffness of the specimen to the test fixture increases. Modeling refinements such as the inclusion of transverse shear should be explored to obtain improved predictive capability. A second boundary condition effect is explored by comparing experimental and numerical results for shells with either free or simply supported axial edges. Shell response prior to bifurcation of the axially free shells is in excellent agreement. In general, however, the response of the axially simply supported shells is more complicated, involving multiple critical points and/or dynamic collapse as well as higher critical loads than shells with free axial edges. These results are important from a design perspective because the simply supported axial edges are a more realistic representation of a fuselage than the free edges, but specimens with free edges are oftentimes used as test articles because of simplicity. The recommendation is made that the effect of other boundary conditions (such as fully clamped) be explored to bound the possible range of responses, particularly in regard to bifurcation and damage resistance.

No damage atypical of that previously observed for composite plates was observed in this work, which is attributed to the lack of observed asymmetric bifurcation modes in cases where the specimens were damaged. Thus, no direct link can be made between asymmetric bifurcation modes and either asymmetric damage at the loading site (which has been already observed) or damage away from the loading site. Further investigation of damage away from the loading site, or asymmetric damage at the loading site, caused by asymmetric (bifurcation) deformation modes can be guided by finite element analyses of shells where bifurcation is predicted. Combined numerical and experimental investigations such as those suggested herein will ultimately lead to a more refined predictive capability for damage resistance of composite structures.

Acknowledgment

This work was sponsored by NASA Langley Research Center under NASA Grant NAG-1-991.

References

[1]Abrate, S., "Impact on Laminated Composite Materials," *Applied Mechanics Review*, Vol. 44, No. 4, 1991, pp. 155–190.

[2]Abrate, S., "Impact on Laminated Composites: Recent Advances," *Applied Mechanics Review*, Vol. 47, No. 11, 1994, pp. 517–544.

[3]Cantwell, W. J., and Morton, J., "The Impact Resistance of Composite Materials," *Composites*, Vol. 22, No. 5, 1991, pp. 55–97.

[4]Palazotto, A. N., Chien, L. S., and Taylor, W. W., "Stability Characteristics of Laminated Cylindrical Panels Under Transverse Loading," *AIAA Journal*, Vol. 30, No. 6, 1992, pp. 1649–1653.

[5]Kistler, L. S., "Experimental Investigation of the Impact Response of Cylindrically Curved Laminated Composite Panels," AIAA Paper 94-1604, April 1994.

[6]Marshall, I. H., and Rhodes, J., "Snap-Buckling of Thin Shells of Rectangular Planform," *Stability Problems in Engineering Structures and Components*, edited by T. H. Richards and P. Stanley, Applied Science Publisher, London, 1979, pp. 249–264.

[7]Wardle, B. L., and Lagace, P. A., "Behavior of Composite Shells Under Transverse Impact and Quasi-Static Loading," *AIAA Journal*, Vol. 36, No. 6, 1998, pp. 1065–1073.

[8]Palazotto, A., Perry, R., and Sandhu, R., "Impact Response of Graphite/Epoxy Cylindrical Panels," *AIAA Journal*, Vol. 30, No. 7, 1992, pp. 1827–1832.

[9]Ambur, D. R., and Starnes, J. H., Jr., "Nonlinear Response and Damage-Initiation Characteristics of Curved Composite Plates Subjected to Low-Speed Impact," AIAA Paper 97-1058, April 1997.

[10]Lin, H. J., and Lee, Y. J., "Impact-Induced Fracture in Laminated Plates and Shells," *Journal of Composite Materials*, Vol. 24, No. 11, 1990, pp. 1179–1199.

[11]Wardle, B. L., and Lagace, P. A., "Importance of Instability in Impact Response and Damage Resistance of Composite Shells," *AIAA Journal*, Vol. 35, No. 2, 1997, pp. 389–396.

[12]Kim, D., and Chaudhuri, R. A., "Full and von Kármán Geometrically Nonlinear Analyses of Laminated Cylindrical Panels," *AIAA Journal*, Vol. 33, No. 11, 1995, pp. 2173–2181.

[13]Chang, T. Y., and Sawamiphakdi, K., "Large Deformation Analysis of Laminated Shells by Finite Element Method," *Computers and Structures*, Vol. 13, No. 1, 1981, pp. 331–340.

[14]Tsai, C. T., Palazotto, A. N., and Dennis, S. T., "Large-Rotation Snap-Through Buckling in Laminated Cylindrical Panels," *Finite Elements in Analysis and Design*, Vol. 9, No. 1, 1991, pp. 65–75.

[15]Talbot, M., and Dhatt, G., "Three Discrete Kirchoff Elements for Shell Analysis with Large Geometrical Non-Linearities and Bifurcations," *Engineering Computations*, Vol. 4, No. 1, 1987, pp. 15–22.

[16]Saigal, S., Kapania, R. K., and Yang, T. Y., "Geometrically Nonlinear Finite Element Analysis of Imperfect Laminated Shells," *Journal of Composite Materials*, Vol. 20, No. 2, 1986, pp. 197–214.

[17]Laschet, G., and Jeusette, J.-P., "Postbuckling Finite Element Analysis of Composite Panels," *Composite Structures*, Vol. 14, No. 1, 1990, pp. 35–48.

[18]Gong, S. W., Shim, V. P. W., and Toh, S. L., "Impact Response of Laminated Shells with Orthogonal Curvatures," *Composites Engineering*, Vol. 5, No. 3, 1995, pp. 257–275.

[19]Kim, S. J., Goo, N. S., and Kim, T. W., "The Effect of Curvature on the Dynamic Response and Impact-Induced Damage in Composite Laminates," *Composites Science and Technology*, Vol. 57, No. 7, 1997, pp. 763–773.

[20]Kwon, Y. S., and Sankar, B. V., "Indentation-Flexure and Low-Velocity Impact Damage in Graphite Epoxy Laminates," *Journal of Composites Technology and Research*, Vol. 15, No. 2, 1993, pp. 101–111.

[21]Sjöblom, P. O., Hartness, J. T., and Cordell, T. M., "On Low-Velocity Impact Testing of Composite Materials," *Journal of Composite Materials*, Vol. 22, No. 1, 1988, pp. 30–52.

[22]Lagace, P. A., Williamson, J. E., Tsang, P. H. W., Wolf, E., and Thomas, S., "A Preliminary Proposition for a Test Method to Measure (Impact) Damage Resistance," *Journal of Reinforced Plastics and Composites*, Vol. 12, No. 5, 1993, pp. 584–601.

[23]Lee, S., and Zahuta, P., "Instrumented Impact and Static Indentation of Composites," *Journal of Composite Materials*, Vol. 25, No. 2, 1991, pp. 204–222.

[24]Jackson, W. C., and Poe, C. C., Jr., "The Use of Impact Force as a Scale Parameter for the Impact Response of Composite Laminates," *Journal of Composites Technology and Research*, Vol. 15, No. 4, 1992, pp. 282–289.

[25]Wu, E., and Shyu, K., "Response of Composite Laminates to Contact Loads and Relationship to Low-Velocity Impact," *Journal of Composite Materials*, Vol. 27, No. 15, 1993, pp. 1443–1464.

[26]Meyer, P. I., "Low-Velocity Hard-Object Impact of Filament-Wound Kevlar/Epoxy Composites," *Composite Science and Technology*, Vol. 33, No. 4, 1988, pp. 279–293.

[27]Manders, P. W., Bader, M. G., Hinton, M. J., and Flower, P. Q., "Mechanisms of Impact Damage in Filament Wound Glass-Fibre/Epoxy-Resin Tubes," *Third International Conference on Mechanical Behaviour of Materials*, edited by K. J. Miller and R. F. Smith, Pergamon, New York, 1980, pp. 275–284.

[28]Wardle, B. L., and Lagace, P. A., "On the Use of Quasi-Static Testing to Assess Impact Damage Resistance of Composite Shells," *Mechanics of Composite Materials and Structures*, Vol. 5, No. 1, 1998, pp. 103–121.

[29]Wardle, B. L., "Buckling and Damage Resistance of Transversely-Loaded Composite Shells," Ph.D. Dissertation, Dept. of Aeronautics and Astronautics, Massachusetts Inst. of Technology, TELAC Rept. 98-7, Cambridge, MA, June 1998.

[30]Tudela, M. A., "Structural Response and Damage Development of Cylindrical Composite Panels," M.S. Thesis, Dept. of Aeronautics and Astronautics, Massachusetts Inst. of Technology, TELAC Rept. 96-11, Cambridge, MA, Sept. 1996.

[31]Wardle, B. L., Lagace, P. A., and Tudela, M. A., "Buckling Response of Transversely Loaded Composite Shells—Part 2: Numerical Analysis," *AIAA Journal* (submitted for publication).

[32]Tudela, M. A., Lagace, P. A., and Wardle, B. L., "Buckling Response of Transversely Loaded Composite Shells," AIAA Paper 98-1992, April 1998.

[33]Bazant, Z. P., and Cedolin, L., "High Arches," *Stability of Structures: Elastic, Inelastic, Fracture, and Damage Theories*, Oxford Engineering

Science Series, Oxford Univ. Press, New York, 1991, pp. 108–118.

[34]Timoshenko, S., "Buckling of Compressed Rings and Curved Bars," *Theory of Elastic Stability*, Engineering Societies Monographs, McGraw–Hill, New York, 1936, pp. 204–238.

[35]Wardle, B. L., "Impact and Quasi-Static Response of Cylindrical Composite Shells," Masters Thesis, Dept. of Aeronautics and Astronautics, Massachusetts Inst. of Technology, TELAC Rept. 95-4, Cambridge, MA, May 1995.

[36]Ranniger, C. U., Lagace, P. A., and Graves, M. J., "Damage Tolerance and Arrest Characteristics of Pressurized Graphite/Epoxy Tape Cylinders," *Composite Materials: Fatigue and Fracture—Fifth Volume*, ASTM STP 1230, American Society for Testing and Materials, Philadelphia, 1995, pp. 407–426.

[37]Wardle, B. L., and Lagace, P. A., "Finite Element Technique for Nonlinear Bifurcation with Application to Shell Structures" (manuscript in preparation).

[38]Lagace, P. A., Brewer, J. C., and Varnerin, C., "TELAC Manufacturing Course Notes," Dept. of Aeronautics and Astronautics, TELAC Rept. 88-4B, Massachusetts Inst. of Technology, Cambridge, MA, May 1988.

[39]Freeman, S. M., "Characterization of Lamina and Interlaminar Damage in Graphite/Epoxy Composites by the Deply Technique," *Composite Materials: Testing and Design*, ASTM STP 787, American Society for Testing and Materials, Philadelphia, 1982, pp. 50–62.

[40]Chang, F. H., Couchman, J. C., Eisenmann, J. R., and Lee, B. G. W., "Application of a Special X-Ray Nondestructive Testing Technique for Monitoring Damage Zone Growth in Composite Laminates," *Composite Reliability*, ASTM STP 580, American Society for Testing and Materials, Philadelphia, 1975, pp. 176–190.

[41]Rankin, C. C., and Brogan, F. A., "An Element-Independent Corotational Procedure for the Treatment of Large Rotations," *Collapse Analysis of Structures: The 1984 Pressure Vessel and Piping Conference and Exhibition*, American Society of Mechanical Engineers, New York, 1984, pp. 85–100.

[42]Crisfield, M. A., *Non-Linear Finite Element Analysis of Solids and Structures*, Vol. 1, Wiley, New York, 1991, pp. 268, 269.

[43]Simo, J. C., Fox, D. D., and Rifai, M. S., "Geometrically Exact Stress Resultant Shell Models: Formulation and Computational Aspects of the Nonlinear Theory," *Analytical and Computational Models of Shells*, edited by A. K. Noor, T. Belytschko, and J. C. Simo, American Society of Mechanical Engineers, New York, 1989, pp. 161–190.

[44]Voyiadjis, G. Z., and Shi, G., "Nonlinear Postbuckling Analysis of Plates and Shells by Four-Noded Strain Element," *AIAA Journal*, Vol. 30, No. 4, 1992, pp. 1110–1116.

[45]Brogan, F. A., Rankin, C. C., Cabiness, H. D., and Loden, W. A., "STAGS User Manual—Version 2.3," Lockheed Martin Missiles and Space Co., Inc., LMMS PO32594, Sunnyvale, CA, July 1996.

[46]Rankin, C., and Brogan, F., "The Computational Structural Mechanics Testbed Structural Element Processor ES5: STAGS Shell Element," Lockheed Missiles and Space Company, Inc., NASA CR-4358, May 1991.

[47]Riks, E., "Some Computational Aspects of the Stability Analysis of Nonlinear Structures," *Computer Methods in Applied Mechanics and Engineering*, Vol. 47, No. 3, 1984, pp. 219–259.

[48]Arbocz, J., "Future Directions and Challenges in Shell Stability Analysis," AIAA Paper 97-1077, April 1997.

[49]Singer, J., "Experimental Studies in Shell Buckling," AIAA Paper 97-1075, April 1997.

[50]Arbocz, J., and Hol, J. M., A. M., "The Role of Experiments in Improving the Computational Models for Composite Shells," *Analytical and Computational Models of Shells*, edited by A. K. Noor, T. Belytschko, and J. C. Simo, American Society of Mechanical Engineers, New York, 1989, pp. 613–640.

[51]Fung, Y. C., and Kaplan, A., "Buckling of Low Arches or Curved Beams of Small Curvature," California Inst. of Technology, NACA TN 2840, Nov. 1952.

[52]Rhodes, J., and Marshall, I. H., "Unsymmetrical Buckling of Laterally Loaded Reinforced Plastics Shells," *Proceedings of the Second International Conference on Composite Materials (ICCM/2)*, edited by B. Noton, R. Signorelli, K. Street, and L. Phillips, Metallargical Society of ASME, Warrendale, PA, 1978, pp. 303–315.

A. N. Palazotto
Associate Editor